Atmospheric potential oxygen: New observations and their implications for some atmospheric and oceanic models

Mark Battle,[1] Sara Mikaloff Fletcher,[2] Michael L. Bender,[3] Ralph F. Keeling,[4] Andrew C. Manning,[4,5] Nicolas Gruber,[2] Pieter P. Tans,[6] Melissa B. Hendricks,[3] David T. Ho,[3,7] Caroline Simonds,[1,8] Robert Mika,[3] and Bill Paplawsky[4]

Received 14 April 2005; revised 10 October 2005; accepted 31 October 2005; published 17 February 2006.

[1] Measurements of atmospheric O_2/N_2 ratios and CO_2 concentrations can be combined into a tracer known as atmospheric potential oxygen ($APO \approx O_2/N_2 + CO_2$) that is conservative with respect to terrestrial biological activity. Consequently, APO reflects primarily ocean biogeochemistry and atmospheric circulation. Building on the work of Stephens et al. (1998), we present a set of APO observations for the years 1996–2003 with unprecedented spatial coverage. Combining data from the Princeton and Scripps air sampling programs, the data set includes new observations collected from ships in the low-latitude Pacific. The data show a smaller interhemispheric APO gradient than was observed in past studies, and different structure within the hemispheres. These differences appear to be due primarily to real changes in the APO field over time. The data also show a significant maximum in APO near the equator. Following the approach of Gruber et al. (2001), we compare these observations with predictions of APO generated from ocean O_2 and CO_2 flux fields and forward models of atmospheric transport. Our model predictions differ from those of earlier modeling studies, reflecting primarily the choice of atmospheric transport model (TM3 in this study). The model predictions show generally good agreement with the observations, matching the size of the interhemispheric gradient, the approximate amplitude and extent of the equatorial maximum, and the amplitude and phasing of the seasonal APO cycle at most stations. Room for improvement remains. The agreement in the interhemispheric gradient appears to be coincidental; over the last decade, the true APO gradient has evolved to a value that is consistent with our time-independent model. In addition, the equatorial maximum is somewhat more pronounced in the data than the model. This may be due to overly vigorous model transport, or insufficient spatial resolution in the air-sea fluxes used in our modeling effort. Finally, the seasonal cycles predicted by the model of atmospheric transport show evidence of an excessive seasonal rectifier in the Aleutian Islands and smaller problems elsewhere.

Citation: Battle, M., et al. (2006), Atmospheric potential oxygen: New observations and their implications for some atmospheric and oceanic models, *Global Biogeochem. Cycles*, *20*, GB1010, doi:10.1029/2005GB002534.

1. Introduction

[2] For more than a decade, concurrent measurements of atmospheric oxygen and carbon dioxide have been used to estimate fluxes of carbon between the atmosphere and the oceans [e.g., *Keeling and Shertz*, 1992]. This approach is possible because most of the processes that result in fluxes of CO_2 to and from the atmosphere also result in fluxes of O_2. Specifically, when fossil fuels are combusted to release 1 mole of CO_2, ~1.4 moles of O_2 will be removed from the atmosphere [*Keeling*, 1988a; *Marland et al.*, 2003]. Similarly,

[1]Department of Physics and Astronomy, Bowdoin College, Brunswick, Maine, USA.
[2]Institute of Geophysics and Planetary Physics and Department of Atmospheric and Oceanic Sciences, University of California, Los Angeles, California, USA.
[3]Department of Geosciences, Guyot Hall, Princeton University, Princeton, New Jersey, USA.
[4]Scripps Institution of Oceanography, University of California, San Diego, La Jolla, California, USA.
[5]Now at School of Environmental Sciences, University of East Anglia, Norwich, UK.
[6]National Oceanic and Atmospheric Administration, Climate Monitoring and Diagnostics Laboratory, Boulder, Colorado, USA.
[7]Now at Lamont-Doherty Earth Observatory, Columbia University, Palisades, New York, USA.
[8]Now at Canaccord Adams, Boston, Massachusetts, USA.

0886-6236/06/2005GB002534$12.00

when a terrestrial ecosystem removes 1 mole of CO_2 from the atmosphere, it also releases 1.1 moles of O_2 [*Severinghaus*, 1995]. The primary exception to this stoichiometric linkage is at the air-sea interface, where substantial O_2 fluxes may be unaccompanied by fluxes of CO_2 and vice versa.

[3] The relationship between atmospheric composition and oceanic O_2 and CO_2 fluxes was elegantly formalized by *Stephens et al.* [1998] (referred to hereinafter as Stephens '98). They defined a tracer, atmospheric potential oxygen (APO) (conceptually, $APO \sim O_2 + CO_2$), which is conservative with respect to terrestrial photosynthesis and respiration. In addition, they effectively removed the combustion signal from APO using records of fossil fuel production. Thus fossil fuel–corrected APO is influenced solely by fluxes of O_2 and CO_2 between ocean and atmosphere. Consequently, precise measurements of O_2 and CO_2 have the potential to provide unique insight into the processes controlling these fluxes and the atmospheric transport that distributes them.

[4] In an effort to realize this potential, Stephens '98, compared their observations of APO with the values derived from runs of several ocean models. They used ocean biogeochemistry models and oceanic heat-flux measurements to predict air-sea CO_2 and O_2 fluxes, and a model of atmospheric transport to turn these fluxes into a spatially and temporally resolved global APO concentration field. This modeled field was then sampled at the station locations and compared with observations. The primary metric for data-model comparison was the north-south gradient in APO. They found substantial discrepancies between model predictions and their observations in both the pole-to-pole gradient and site-to-site gradients within each hemisphere. These discrepancies persisted regardless of the choice of ocean biogeochemistry model. Stephens '98, concluded that the ocean models appeared to underestimate the southward transport of summed O_2 and CO_2 in the oceans, perhaps indicating an underlying deficiency in the models' representation of ocean physics. Furthermore, all of the models predicted a substantial equatorial maximum in APO. Unfortunately, this distinctive model bulge could not be verified owing to the absence of equatorial APO data.

[5] The connection between air-sea gas fluxes and APO was revisited by *Gruber et al.* [2001], (referred to hereinafter as Gruber '01) who developed an inversion technique to estimate annual mean net air-sea fluxes of O_2. They used observations of dissolved oxygen and related tracers in the oceans and OGCMs to infer fluxes that were independent of both air-sea gas-exchange parameterizations and models of nutrient cycling in the oceans. Nonetheless, their O_2 flux estimates remained dependent on accurate representations of ocean physics in the OGCMs employed in their inversions.

[6] Like the earlier study, Gruber '01 then used a model of atmospheric transport, along with observationally based estimates of CO_2 fluxes and heat fluxes, to convert their air-sea O_2 fluxes into predictions of APO at various locations. These predictions were then compared with observations of APO made by *Stephens* [1999] (referred to hereinafter as Stephens '99). The comparison was evaluated with the same metric as Stephens '98: the north-south gradient. Gruber '01 found that the data-model disagreement was reduced, but still significant, and did not appear to point to a problem with modeled southward oceanic transport. The equatorial bulge remained a prominent feature of the modeled APO gradient. Furthermore, Gruber '01 found that their predictions of the APO gradient were largely independent of the particular ocean physics model used in the inversion. They suggested that their data-model discrepancies might be due in part to deficiencies in their model of atmospheric transport. They also emphasized that a stringent test of their model predictions would require a long-term record of APO in the tropics (data which still did not exist at the time of publication) and a greater density of observations at high latitudes.

[7] Like Stephens '98 and Gruber '01, we primarily examine two aspects of the north-south APO gradient: the interhemispheric gradient, and the equatorial bulge. While intrinsically interesting, each of these aspects address outstanding questions in other areas.

[8] The interhemispheric APO gradient arises from the combination of three large-scale processes: the uptake and release of O_2 and CO_2 by high-latitude oceans, the transport of O_2 and CO_2 from north to south by the abyssal circulation of the ocean, and the redistribution of these air-sea fluxes by interhemispheric mixing of the atmosphere. Consequently, an understanding of the interhemispheric APO gradient will illuminate the role of the oceans in determining the atmospheric CO_2 gradient. In turn, this improves our ability to quantify the size and distribution of terrestrial carbon fluxes [*Keeling et al.*, 1996].

[9] The size and extent of the equatorial bulge in APO is a direct indicator of the vigor with which water upwells at the equator. Waters upwelling at the equator are cold and rich in dissolved CO_2, resulting in a flux of CO_2 to the atmosphere that is enhanced by warming. The upwelling waters are undersaturated in O_2, leading to a flux of that gas into the oceans. However, the waters are also nutrient rich. The resulting net production transfers more O_2 to the air than is consumed by respiration, and also causes a net transfer of CO_2 from the air to the ocean. The sum of all of these fluxes results in a pronounced equatorial bulge in APO, with more equatorial upwelling leading to a more pronounced equatorial bulge. Thus the structure of APO concentrations near the equator provides a firm constraint on upwelling and ocean energetics.

[10] In this paper, we use the simplified definition of APO adopted by Gruber '01,

$$\mathrm{APO} = \delta O_2/N_2 + 1.1 \times 4.8 \times [CO_2],$$

where $[CO_2]$ is given in ppm and APO and $\delta O_2/N_2$ are given in "per meg" (1 per meg = 0.001). The factor of 1.1 represents the average stoichiometric ratio of O_2 to CO_2 for terrestrial ecosystems [*Severinghaus*, 1995] and 4.8 converts from ppm to per meg, since 20.9% of the atmosphere is O_2. This equation is slightly simplified from the original definition of Stephens '98 since it ignores oxidation of CH_4 and CO; processes which have a negligible impact on APO gradients Stephens '98.

[11] We now present an expanded set of APO observations, combining data from the sampling networks operated independently by Princeton University (PU) and the Scripps Institution of Oceanography (SIO). The data set includes

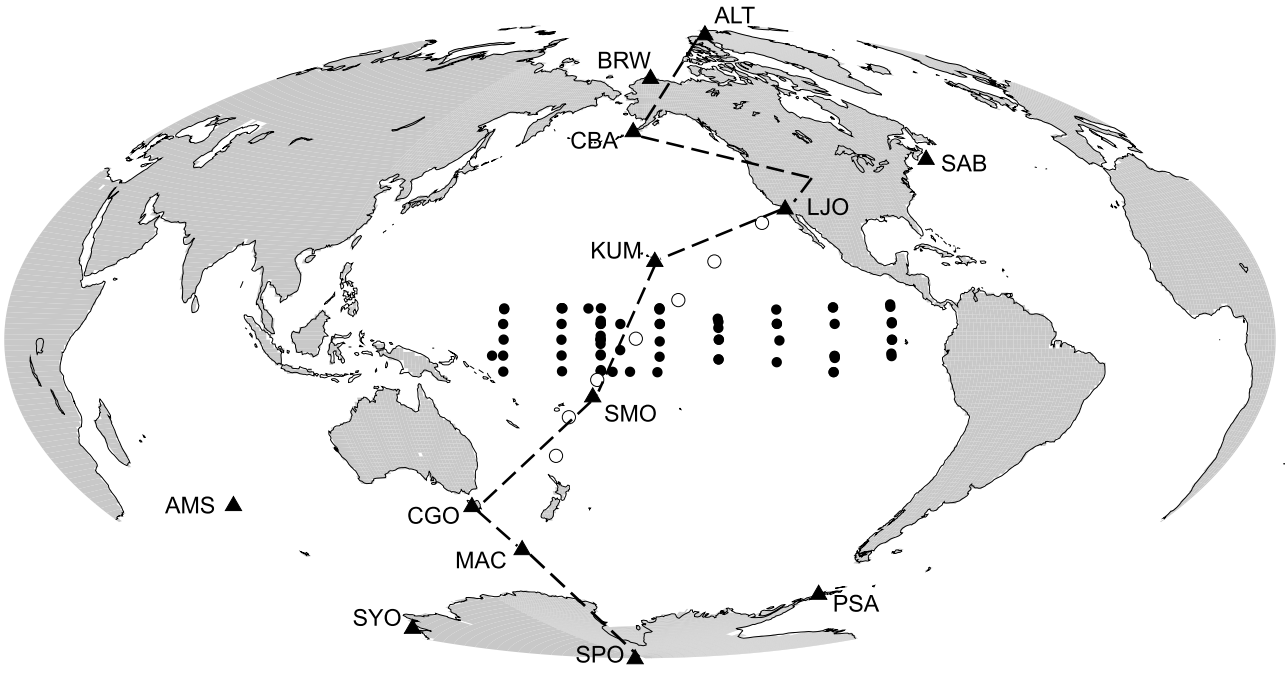

Figure 1. Locations at which O_2/N_2 and CO_2 samples were collected for use in this study. Solid triangles indicate land-based stations, solid circles show sampling locations for the NOAA ship Ka'imimoana, and open circles show sampling locations for the Blue Star freighters. The dashed line shows the transect used by *Gruber et al.* [2001], and referenced in Figure 7 of this paper.

new records of APO from the tropics. In the sections that follow, we present the methods of sample collection and analysis. We then describe two different methods for deriving north-south gradients from our data set, and discuss our observations. The penultimate section presents an updated version of the Gruber '01 method, and its predictions of APO. Finally, we compare the model predictions to our observations and discuss the possible origins of the remaining data-model differences.

2. Sample Collection and Analysis

[12] The locations of the SIO and PU sampling stations used in this study are shown in Figure 1. Several stations for which the SIO and PU programs have data are omitted from this study, for reasons including limited duration of the records and sampling outside the planetary boundary layer.

2.1. Scripps Protocols

[13] The collection and analysis protocols for the SIO program have been published in detail [*Keeling et al.*, 1998; *Keeling*, 1988a]. In brief, samples of dried, whole air are collected biweekly in triplets of 5-L glass flasks filled to 1 bar. The filled flasks are returned to Scripps, where they are analyzed for O_2/N_2 ratios using an interferometric method [*Keeling*, 1988b]. The same gas stream is analyzed for CO_2 using a nondispersive infrared (NDIR) analyzer [*Keeling et al.*, 1998]. More recently, an isotope ratio mass spectrometer has been added to the analysis system. Part of the sample (and reference) gas stream is diverted to this instrument and analyzed for Ar/N_2, as well as other species [*Keeling et al.*, 2004]. Mass spectrometric Ar/N_2 data are included in the SIO data set from mid-2001 forward.

2.2. Princeton Protocols

[14] The collection and analysis protocols for the PU program have also been published [*Bender et al.*, 1994, 1996, 2005; *Battle et al.*, 2000]. Samples comprising the PU data set fall into two categories: those collected at land-based stations and those collected on ships. For both categories, duplicate samples of dried air are collected in 2-L glass flasks filled to 1 bar. The flasks are returned to Princeton University for analysis with an isotope ratio mass spectrometer. Two or three aliquots (of ~100scc) are removed from each flask and analyzed for O_2/N_2 and Ar/N_2 ratios [*Bender et al.*, 2005]. The flasks are then sent to NOAA/CMDL in Boulder, Colorado, where the CO_2 mixing ratio of the remaining air is measured with an NDIR analyzer [*Conway et al.*, 1994]. At our land-based stations, samples are collected either weekly or biweekly, during periods believed to be free of local influences. The details of the collection systems (pumps, valves, drying traps, flow rates) are very similar to those used to collect the SIO samples [*Keeling et al.*, 1998].

[15] Shipboard collections of samples were begun by PU in 1996 on ships of opportunity sailing in the Pacific Ocean. Between 1996 and 2001, samples were collected on commercial container ships operated by Blue Star Line (which was later acquired by P&O Nedlloyd). From 1996 until 1998, samples were collected by the crew of the Brisbane Star, sailing between Los Angeles, California, and Aukland, New Zealand, via Suva, Fiji. The sampling equipment was

then moved to the Argentina Star, which was in service on that route until late in the year 2000. Samples were collected at exact 10° latitude lines from 30°N to 30°S, along the transect illustrated in Figure 1.

[16] Since May of 2001, PU shipboard samples have been collected by the scientific personnel on the NOAA research ship Ka'imimoana. This vessel regularly services the TOGA/CORE moorings in the Equatorial Pacific. Moorings are located along meridians between 162°E and 95°W. Samples were collected while the ship was underway along mooring meridians, at nominal intervals of 4° in latitude between 8°N and 8°S. The exact sampling locations are shown as small crosses in Figure 1.

[17] On both the Brisbane Star and the Ka'imimoana, samples were collected through a single 3/8″ (O.D.) Dekoron™ line with the intake located at the top of the foremast on the bow of the ship. On the Argentina Star, samples were collected through one of a pair of 3/8″ Dekoron™ lines with the intakes on the port and starboard wings of the bridge. The officer on duty selected the line which was windward at the time of sampling.

[18] Shipboard samples were collected using automated systems designed to standardize sample collection and minimize reliance on the operators. A computer running LabView™ was responsible for recording location and time of collection (via a GPS interface), monitoring flow rates and flushing times, controlling temperatures of the cryogenic trap, activating the pump, purging the water trap, and prompting the operator for input when appropriate. The operators were responsible for initiating the sampling cycle at the appropriate locations and swapping flasks after collections were complete. On the first-generation sampler used on the Blue Star freighters, the operator was also prompted to open and close flasks. In all other respects, the shipboard samplers were equivalent to those used at the PU and SIO land sites [*Keeling et al.*, 1998].

2.3. Correcting Data for Sampling Biases Using Ar/N_2

[19] We intend to use the climatological APO gradients from site to site to gain insight into biogeochemical processes and model shortcomings. Consequently, it is essential that our samples faithfully represent the atmospheric composition at the time of collection (or are biased in exactly the same way at all sites).

[20] If the SIO and PU collection or analysis protocols introduce different biases system wide, the empirical detrending process will take care of the problem (see section 3.1). However, if the sampling systems at different sites within a network were to introduce different collection biases, we would infer a spurious gradient between these sites. One example of such a site-specific bias is thermal fractionation at the point of collection [*Manning*, 2001]. The expression of the fractionation could depend on flow rates, intake geometry and other site-dependent parameters.

[21] Our best tool for quantifying site-to-site biases is the set of Ar/N_2 measurements made on the same flasks for which APO is calculated, since many of the processes that fractionate Ar/N_2 also fractionate O_2/N_2, and by extension, APO. If the processes are mass dependent, fractionation will occur in the ratio of 3:1 (Ar/N_2 to O_2/N_2). Thermal fractionation was examined in detail by *Keeling et al.* [2004]. These authors measured a divided gas stream in the presence of a thermal gradient at 1 atmosphere of pressure, and found that Ar/N_2 values were fractionated 3.77 ± 0.04 times as much as O_2/N_2 values. They also found a clear pressure dependence in this number.

[22] Since we cannot know which processes are influencing our collections, we empirically determine the relative fractionation of Ar/N_2 and O_2/N_2 using data from Cape Grim. At this site, we collect Princeton samples simultaneously on two completely independent sampling systems: the original manual unit (operating since 1992) and a shipboard-style automated system (commissioned in Sept. 2001). Pairs of flasks are filled on both systems. Systematic differences between the pairs must be introduced by the different sampling methods, while simple scatter may be attributed to sampling and laboratory errors.

[23] Average values of the manual-automated differences ($O_2/N_2 = 2.8 \pm 0.9$ and $Ar/N_2 = 13 \pm 3$) show that some of the fractionation is originating with one or both samplers, since laboratory analysis artifacts would simply cause scatter about zero. A fit to the difference data shows that Ar/N_2 and O_2/N_2 are fractionated in the ratio 3.3 ± 0.3:1 (see Figure S1 of the electronic supplement[1]). This value is consistent with both mass-dependent and thermal fractionation, within errors.

[24] On the basis of modeling studies [*Keeling et al.*, 2004], we expect the annual mean atmospheric Ar/N_2 ratios at our sites to span a range of roughly 5.3 per meg, with most sites lying within a range of 2 per meg. It remains possible that values at polar sites may be higher owing to the interaction of winter inversions and gravitational fractionation [*Keeling et al.*, 2004]. With this in mind, we assume that any site-to-site gradients in Ar/N_2 present in our data in excess of $\sim$2 per meg are due to collection biases.

[25] Our measured annual mean values of Ar/N_2 are given in auxiliary materials Table S1. Most of the values cluster within a small range, suggesting zero or constant fractionation. However, some show clear signs of sampling bias. Macquarie is the most noteworthy example, differing from the nearest stations (Cape Grim and Syowa) by as much as 42 per meg.

[26] On the basis of the arguments just presented, we correct our APO data set for sampling artifacts by subtracting $0.30 \times \delta Ar/N_2$ from the observed APO values, where $\delta Ar/N_2$ refers to the annual average Ar/N_2 value calculated for each site (see auxiliary material Table S1). We apply a single correction for both the Brisbane Star and Argentina Star, as the same equipment was used on both vessels. The sizes of the corrections are shown in panel 1 of Figure 2. Assuming that the true spatial variability in annually averaged Ar/N_2 is $\leq$2 per meg, our corrections introduce an error <1 per meg in annually averaged O_2/N_2. Except where otherwise noted, we always refer to corrected O_2/N_2 in the ensuing discussion.

[1] Auxiliary material is available at ftp://ftp.agu.org/apend/gb/2005GB002534.

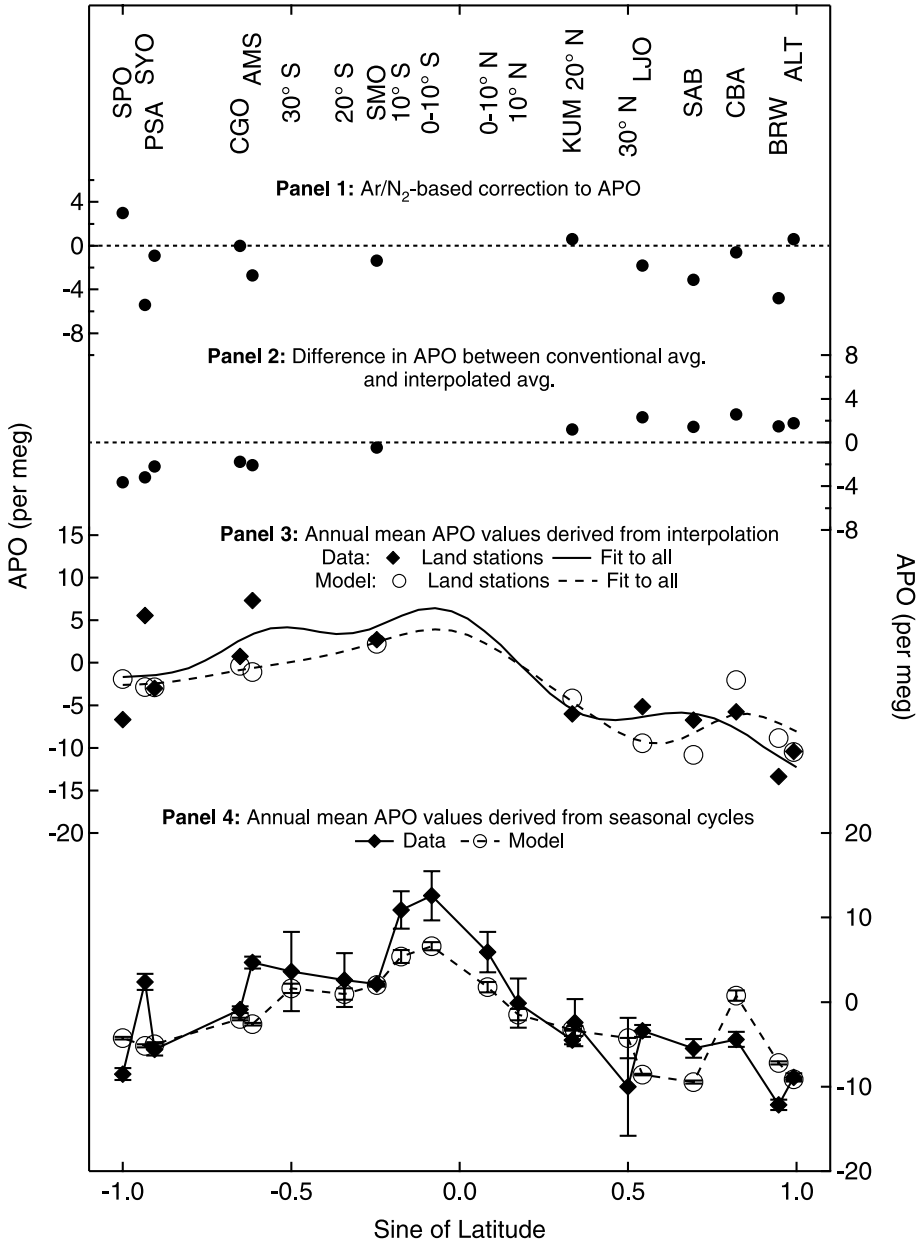

Figure 2. North-south gradients in APO. Panel 1 shows the amount subtracted from measured APO values at each land-based sampling location to correct for aliasing during sample collection. Values are derived from measured Ar/N_2 values. For details, see section 2.3 and auxiliary material Table S1. Panel 2 shows the impact of the temporally uneven weighting used in calculating annual mean values of APO in the two-dimensional interpolation scheme described in section 3.2. Negative values imply that conventional averages are lower than interpolated averages. Panel 3 shows the gradients in annually averaged APO calculated using this interpolation method, for both observations and model output. All data are Ar/N_2 corrected. Model output has been processed in exactly the same manner as data. The spatial interpolation (solid and dashed lines) are averages of Butterworth filter fits to the land stations (shown as points) and to the spatially unbinned shipboard measurements (not shown). See section 3.2 for details. Panel 4 shows gradients in annually averaged APO derived from sinusoidal fits of the seasonal cycles at land stations and spatially binned shipboard data. All data are Ar/N_2 corrected. Model output has been processed in exactly the same manner as the data. Lines between points simply guide the eye. Error bars indicate only the statistical uncertainty associated with the offsets of the sinusoidal fits. For details, see section 3.3 and auxiliary material Table S2. Zero-points in panels 3 and 4 reflect the average of the annual means at CGO and SMO, determined using the methods of *Thoning et al.* [1989]. The zero-point of the model output is arbitrary, so all model results have been shifted to aid visual comparison with data.

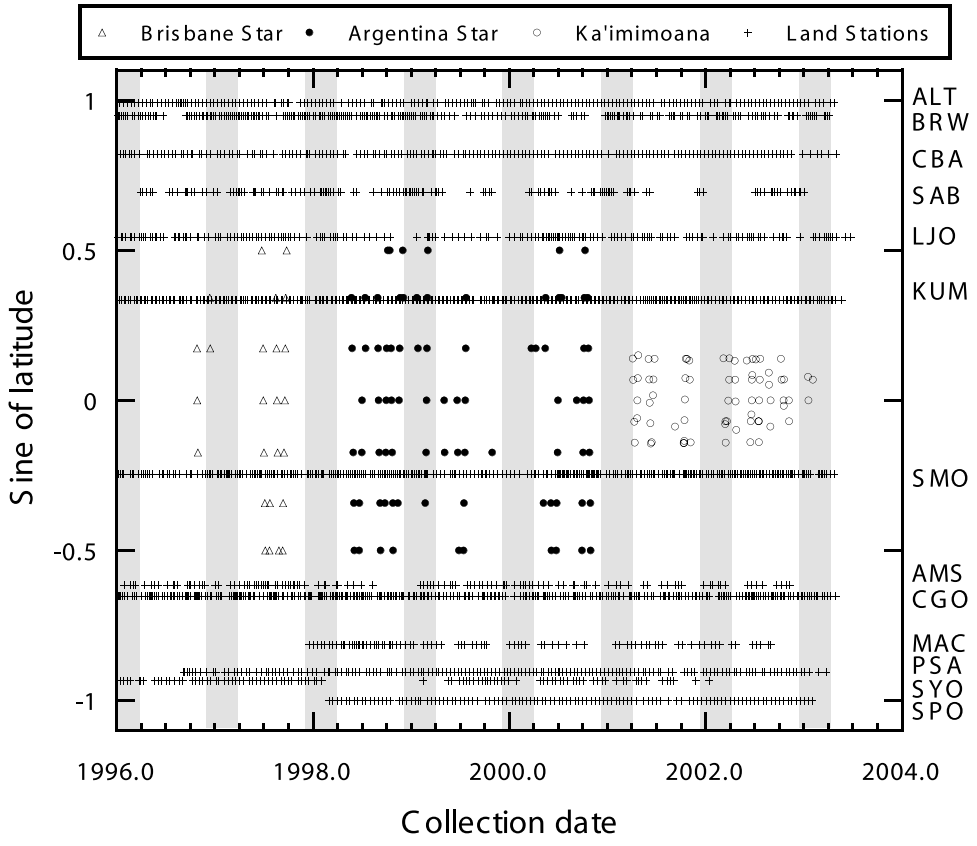

Figure 3. Locations in time and latitude of the samples used in this study. Periods corresponding approximately to the boreal winter are indicated with gray bands.

2.4. Rejected Data

[27] Criteria for rejecting individual samples or replicate pairs/triplets are discussed by *Keeling et al.* [1998] and *Bender et al.* [2005]. In addition, we choose to omit four more subsets of the data from further consideration.

[28] 1. We believe the climatological APO value we measure at Macquarie (MAC) is untrustworthy. Unlike other sites with dedicated intake lines, the MAC samples were subsampled from a central shared line, providing ample opportunity for fractionation [*Manning*, 2001; *Battle et al.*, 2003; *Keeling et al.*, 2004]. The very low annual mean value of Ar/N_2 clearly points to a large sampling artifact in O_2/N_2 and the required Ar/N_2 correction would be accompanied by an unacceptably large uncertainty. While the last three pairs of flasks collected aboard the Ka'imimoana require an Ar/N_2 correction comparable to MAC, we choose to retain these data because the earlier data from this platform provide a consistency check on these highly corrected values.

[29] 2. We omit data collected at SPO prior to 1998. *Manning* [2001] has shown that the long-term subfreezing storage of samples collected at SPO in the years 1991–1997 biased those data by 10 per meg or more.

[30] 3. We omit samples collected at Syowa (SYO) between mid-January 1998 and mid-January 1999. O_2/N_2 and CO_2 values in our flasks are anomalous during this period, and CO_2 values in NOAA-CMDL flasks collected during this period are also problematic [*Bender et al.*, 2005].

[31] 4. We use an iterative technique to eliminate outliers from the prevailing data envelope in the PU data set. Climatological records at each station (see section 3.1) are fitted with a smooth curve [*Thoning et al.*, 1989] and residuals to the curve are calculated. Those data more than 4.0 σ from the curve are cut and the retained data are refitted. This sequence of steps is repeated until no further data are eliminated. As a result of this process, 16 sample pairs at SAB were cut (120 retained), along with four pairs from the Blue Star ships.

[32] All data meeting these criteria are available in the auxiliary material.

3. Calculation of North-South APO Gradients

[33] The APO data set described above is unprecedented in its temporal and spatial coverage. Nonetheless, it remains sparse in both senses. Figure 3 shows sampling as a function of time and latitude. Despite having much longer records at some sites than shown here, we restrict our data set to the period starting in January of 1996 when our shipboard collections commenced. We also recognize that the structure of the APO field will change from year to year. These changes will be due to interannual variability in both the oceanic processes leading to air-sea APO fluxes

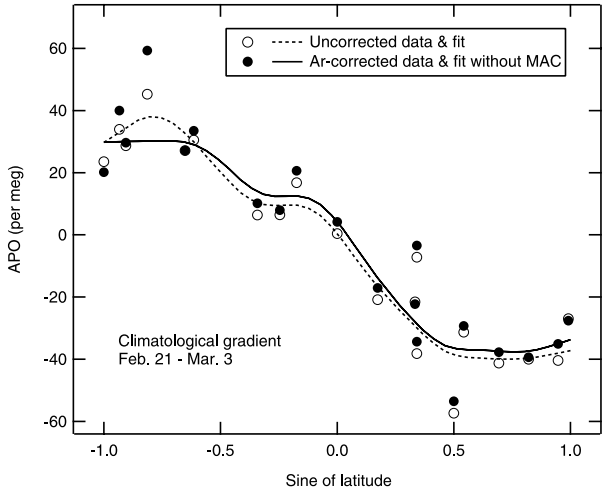

Figure 4. An example of a single time slice of APO, corresponding to an 11-day period beginning on 21 February of the climatological year. Data (means for all samples at a site collected within the designated time interval) are shown with and without Ar/N2 correction, along with a Butterworth filter fit to the measurements. Macquarie is included in this plot, but excluded from the Ar-corrected fit.

and in the atmospheric transport that carries those fluxes to the points of observation. Since our goal is to focus on the long-term mean north-south APO gradient, we wish to reduce the impact of this interannual variability. To do so, we compress our 7-year record into a single climatological year.

[34] Even with more than 7 years of data, the shipboard records do not cover the climatological year evenly. Owing to untimely changes of vessels and malfunctioning hardware, there is a paucity of data covering the boreal winter (see the gray bands in Figure 3).

[35] With this limitation in mind, we calculate north-south gradients in APO as follows: (1) detrend all records using a single temporal trend; (2) collapse records into a single climatological year; (3) determine annual mean values for each station/latitude using either interpolation or a seasonal fitting procedure; and (4) correct data for sampling biases using Ar/N_2. These steps are described in detail in the subsections that follow.

3.1. Detrending and Creation of a Climatology

[36] Determining the climatological gradient of APO using both the PU and SIO data sets presents two complications. First, APO exhibits a secular decrease, due to the net effects of oceanic and fossil fuel uptake and release of O_2 and CO_2. In order to reduce the 7-year time series into a single climatological year, we need to remove this trend. Second, the SIO and PU data sets of O_2/N_2 are each referenced to an arbitrary standard that is unique to the home laboratory [*Keeling et al.*, 1998; *Bender et al.*, 1996].

[37] We can address both of these complications by determining the gradients relative to the two sites common to the PU and SIO networks: Cape Grim, Tasmania (CGO) and American Samoa (SMO). We first determine trends from the data collected by each lab at CGO and SMO. These trends are determined using the method of *Thoning et al.* [1989], whereby records are fitted with the sum of a third-order polynomial, four harmonics and filtered residuals. The polynomial and those residuals with periods of greater than 12 months define the trend. The two trends are averaged for each laboratory, and subtracted from all time series of the respective labs. Because the SIO and PU programs measure CGO-SMO gradients that differ by less than 1 per meg, this method of detrending effectively places the two sampling networks on the same scale. Once the trends have been removed from all of the records, we retain only the month and day of collection (discarding the year), thereby creating a climatology of both the seasonal cycle and annual mean values of APO at each station, all referenced to a virtual station with a mean value halfway between those of CGO and SMO.

3.2. Annual Mean Values From Interpolation

[38] As discussed above, the data set has limited spatial coverage and substantial temporal unevenness. One way to construct north-south gradients in the face of these limitations is to treat the coordinate grid as two-dimensional (sin(latitude) and time) and interpolate to regularly spaced values on this grid.

[39] To carry out this interpolation, we begin by dividing the climatological data set into a series of 35 nonoverlapping "time slices," each of which corresponds to one of the ~2-week periods over which a ship completed a northbound or southbound transit. Each time slice contains a common set of land sampling sites, but a different set of shipboard locations. To make all time slices comparable, we interpolate between the sampling sites of each time slice with a Butterworth filter [*Tans et al.*, 1989]. In the fitting process, land station data are weighted twice as heavily as oceanic data, reflecting their much greater data density (Figure 3). In practice, this weighting has little impact since most oceanic data are quite distant from the land stations. A single representative time slice is shown in Figure 4, demonstrating that the fitting algorithm provides a reasonable and objective method of filling the spatial gaps in the data. The standard deviation of the residuals to these fits is ±5.1 per meg.

[40] With spatial interpolation complete, we use fits of the 35 time slices to determine the annually averaged gradient in APO. Since the time slices (and their corresponding fits) are spaced unevenly through the year, the fits must be weighted to give something close to a conventional annual mean value. To derive weights for the time slices, we use the results of Gruber '01 for guidance. Monthly APO profiles from this method show that during some months (e.g., March–May) the APO profile is roughly static, while during other months (e.g., June), the profile is changing rapidly. On the basis of this behavior, we divide the year into five temporal "bins": December–February, March–May, June, July–October, November. Longer bins correspond to slower changes in the APO profile. We then place

the 35 fitted time slices into the appropriate bins with $n = 3$, 8, 3, 17 and 4 time slices in the respective bins. We calculate average APO for each bin, and then average the bins with relative weights 3:3:1:4:1, respectively. We adopt this approach in order to compare our work as easily as possible with the earlier work of Stephens '98 and Gruber '01. Results of this two-dimensional interpolation are shown in panel 3 of Figure 2.

[41] Panel 2 of Figure 2 shows differences between annual average APO determined using this interpolation scheme, and conventional annual averages calculated using the method of *Thoning et al.* [1989] (essentially identical to that of Gruber '01). While the two methods give similar results, interpolated values are systematically higher (lower) than conventional averages at Southern (Northern) Hemisphere stations. These differences are due to the limited number of collections in the December–February bin. By chance, the collections that do exist in this bin coincide almost exactly with the peak (trough) of the APO cycle in the Southern (Northern) Hemisphere. Therefore a conventional average of a bin will be lower than the one we calculate with our limited number of collections if the station is in the Southern Hemisphere, and higher if the station is in the Northern Hemisphere.

3.3. Annual Mean Values From Seasonal Cycles

[42] We also consider an alternative approach to constructing north-south gradients from sparse data. We divide the shipboard data into 8 groups: 30°, 20°, 10° N and S, 0–9°N, and 0–9°S. For each group we calculate a seasonal cycle with a constant offset. These offsets are the annual mean values for each interval.

[43] To calculate the seasonal cycle for each group, we start with an updated version of the Gruber '01 method (described below) to model a seasonal cycle for each of these groups. The longitudes at which we model the seasonal cycle are taken from the transect of Stephens '98, and are averaged north-south across the latitude interval for the two equatorial bins. The modeled cycle is fitted with a simple sine wave with period of 1 year. This gives an amplitude and phase for each group. Finally, we fit all of the detrended shipboard data in each group with a sine wave plus offset. The amplitude and phase of the sine wave are fixed to the model predictions, and the period is set to 1 year, so that only the offset (i.e. annual mean) is allowed to vary. These annual mean values are shown in panel 4 of Figure 2. Complete results of these sine fits are given in auxiliary material Table S2.

[44] Determining the offsets at the land stations is comparatively easy. For consistency, we fit the climatology of APO at each station with a simple sine wave of fixed period (1 year). Amplitude, phase and offset are all optimized. These offsets for the land stations (i.e., annual mean values) are also shown in panel 4 of Figure 2. Although the seasonal cycles at some stations are clearly not well represented by a simple sine wave (see Figure 5), this method yields annual averages for the land stations that are very close to values determined using the widely accepted method of *Thoning et al.* [1989]. The mean difference between the values from simple sines, and those from the Thoning et al. method is 0.1 ± 0.7 per meg with a maximum difference of 1.8 per meg (n = 13 stations).

4. Discussion of Data

[45] Annually averaged APO values show clear spatial structure, with a maximum at the equator (See panels 3 and 4 of Figure 2). The interhemispheric gradient is weak: stations poleward of 40° have similar values in the two hemispheres. Superimposed on these large-scale features is a significant amount of small-scale structure. Examples include differences of Barrow from Cold Bay, Amsterdam from Cape Grim, and Syowa from both Palmer and South Pole. East-west variability undoubtedly contributes significantly to these gradients. Stations at similar latitudes may derive air from very different regions. For example, back-trajectory analysis (www.cmdl.noaa.gov/ccgg/iadv) indicates that air at Palmer originates from the Southern Ocean (mostly the Pacific Sector), whereas air at Syowa is largely katabatic, spilling off the polar plateau.

[46] Hidden in the climatologies of the meridional gradients is significant temporal variability. Figure 6 shows the APO annual mean gradients between Cape Grim and Alert (SIO data) and Cape Grim and Barrow (Princeton data), as a function of time. Both of these north-south gradients show temporal changes, with peaks and troughs in the Alert record that may be present in the Barrow record, lagged by a few months. The time dependence of these and other gradients is most likely due to changes in oceanic O_2 and CO_2 fluxes, with some contribution from interannual variability in atmospheric transport. Model studies [*Keeling et al.*, 1996] show changes in fossil fuel combustion will have a very small impact on APO gradients. Also shown in Figure 6 are the time periods covered by the analyses of Stephens '98 and Stephens '99, revealing that even with five or more years of data in hand, time-averaged APO gradients evolve, and comparisons of different analyses must be made with care. Our results are qualitatively consistent with recent APO measurements made in the western Pacific [*Tohjima et al.*, 2003].

[47] In summary, there are geochemically significant zonal and temporal gradients in APO, as for CO_2. Here we focus on large-scale, time-averaged gradients for the years 1996.0–2003.0; temporal and regional scale variability will be considered elsewhere.

5. Modeling

[48] In order to begin understanding the processes that lead to the patterns of APO that we observe, we have employed an updated version of the modeling approach of Gruber '01. Our method is conceptually identical to the work of Gruber '01, although some of the component models and boundary conditions are different, as summarized in Table 1. Global fossil fuel CO_2 emission data from *Marland et al.* [2003] were only available through 1999. We assumed that for the year 2000, these emissions were 6.6 PgC/yr and rose by 0.1 Pg/yr thereafter (T. Boden, personal communication, 2004). These emissions were spatially distributed according to the 1995 pattern from the Carbon Dioxide Information Analysis Center, prepared by

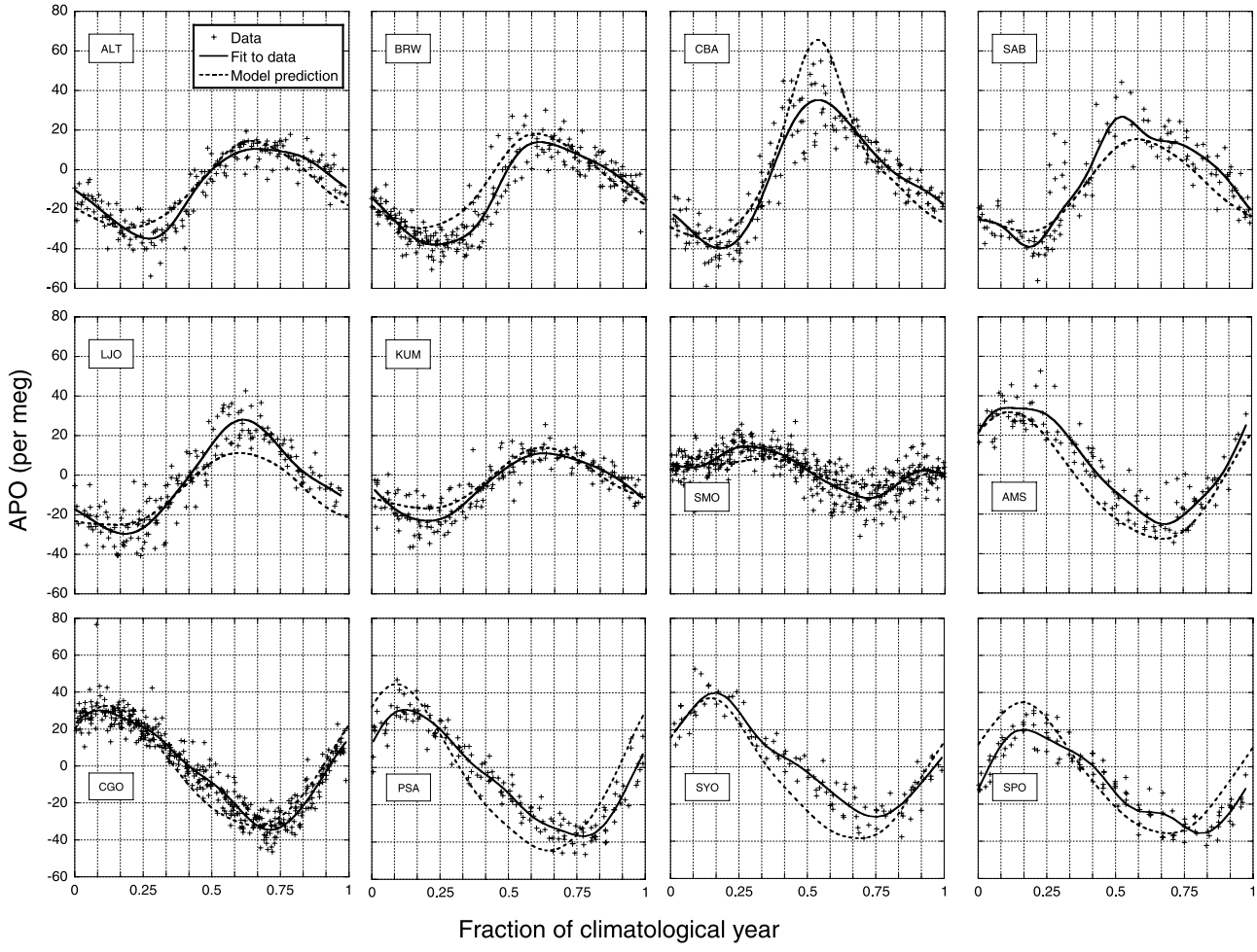

Figure 5. Climatological seasonal cycles of APO at the land-based sampling sites. Observations and fits [*Thoning et al.*, 1989] are shown with crosses and solid lines, respectively. Equivalent fits to model output are shown with dashed lines. Note that the annual means of these cycles are not zero, reflecting the spatial gradients in APO discussed in body of the text.

Antoinette Benkert (http://cdiac.esd.ornl.gov/ndps/ndp058a.html). Fossil CO_2 has an impact on the spatial gradients of APO. However, the model output is largely insensitive to the time dependence assumed for the emissions, since the model output (like the observations) is detrended before gradients are calculated. The O_2 fluxes from fossil fuel were derived from the CO_2 fluxes simply by scaling by a factor of -1.40. This factor is the time- and space-averaged stoichiometric ratio of O_2 to CO_2 appropriate for the current mix of fossil fuels and cement manufacturing. For our purposes, variations in this number are negligibly small [*Keeling*, 1988a; *Marland et al.*, 2003].

[49] For this study, we employed the atmospheric transport model Tracer Model version 3 (TM3) [*Heimann and Körner*, 2003]: a 3-D Eulerian model driven by offline wind fields. All of the input fluxes were aggregated to the TM3 grid and interpolated in time following the Transcom 3 protocol [*Gurney et al.*, 2000].

[50] In contrast to this study, Gruber '01 used the Global Chemical Transport Model (GCTM) [*Mahlman and Moxim*, 1978]. Relative to GCTM, TM3 has a longer interhemispheric exchange time [*Denning et al.*, 1999] and a stronger seasonal rectifier [*Gurney et al.*, 2003].

[51] Because TM3 is driven by analyzed winds, our model results are potentially subject to the impact of interannually varying atmospheric transport. The modeled annual mean APO values at most stations vary by $\sim$2 per meg or less owing to transport, but near the equator APO may vary by as much as 5 per meg from year to year. The gradients between high northern and high southern latitudes vary by less than 3 per meg. To reduce this impact, we created a climatology with multiple model runs, each with repeating National Center for Environmental Prediction (NCEP) winds [*Kalnay et al.*, 1996]. More specifically, the model was run for 10 years (with input fluxes appropriate for the years 1995–2004) with 1995 repeating winds, and the output was saved. Subsequent 10-year runs were performed with repeating winds from 1996, 1997, 1998, 1999 and 2000. Finally, for each of the 10 model years, output from the six multiyear runs were averaged to create a climatology.

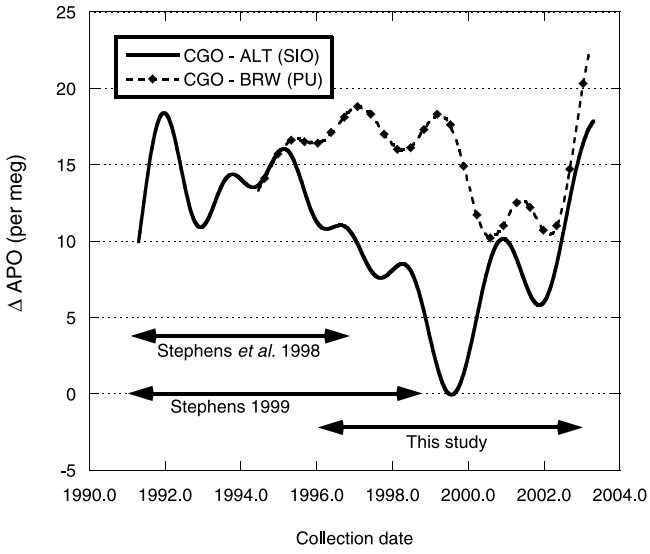

Figure 6. Gradients in APO between Alert and Cape Grim (from SIO) and between Barrow and Cape Grim (from PU) as a function of time. The traces represent running 12-month averages. Also shown are the time periods used in the analyses of Stephens '98, Stephens '99, and this study.

[52] In order to mimic our sparse data set, we recorded biweekly, instantaneous model mixing ratios in the grid cells corresponding to the locations of the land stations. To emulate the shipboard observations, we recorded instantaneous mixing ratios sharing exactly the same space-time coordinates as our (sparse) observations.

[53] This final set of model output was analyzed in exactly the same fashion as our observations (following the steps described in sections 3.2 and 3.3). As with our observations, the analysis begins in model year 1996, thereby discarding the spinup period (model year 1995). Note also that the reference point on the scale (of both the model and the data) is completely arbitrary. Therefore, in the plots showing both model and data, we have shifted the zero-point of the model output so that the comparison with the observations is visually clear.

6. Data-Model Comparison

[54] Model gradients derived using both the interpolation method and seasonal cycles are shown in panels 3 and 4 of Figure 2. Two features are immediately apparent: the model successfully reproduces the observed interhemispheric gradient in APO, and the equatorial "bulge" in APO appears slightly larger in the observations than in the model. This is in clear contrast to the earlier studies of Stephens '98 and Gruber '01, where the models underestimated the magnitude of the interhemispheric gradient and showed an equatorial bulge that appeared to be much larger than allowed by the limited data available at the time.

[55] While the interhemispheric difference and the equatorial bulge dominate the north-south gradient in APO, there are other features in the data that the model does not capture particularly well. For example, the modeled APO values are low at LJO and SAB and high at CBA (relative to the observed and modeled KUM-ALT gradient). In the sections that follow, we examine these and other aspects of the data-model comparison in more detail.

6.1. Interhemispheric Gradient

[56] At first glance, it appears that the model does an excellent job of predicting the observed interhemispheric gradient in APO. In contrast, modeling work of Stephens '98 and Gruber '01 differed substantially from observations. We observe good agreement because the gradient has evolved to match the model prediction (discussed in section 4).

[57] Nonetheless, the interhemispheric gradients predicted by the various models do show significant differences. Stephens '98 found an SPO-ALT difference ranging from -1 to 4 per meg. Gruber '01 found a range of 10 to 12 per meg, depending on model details. Our model predicts an SPO-ALT difference of 6 or 9 per meg (depending on the method we use for calculating the annual average). The source of these changes is difficult to determine, since each study uses a different model of atmospheric transport and a different set of input fluxes. In addition, there is the question of study period: while oceanic input fluxes are determined from data sets which are effectively steady state, the input fossil fuel fluxes do reflect the varying periods over which the models are compared to the data.

[58] In this paper, we limit our comparison to the differences between the Gruber '01 study and our own modeling work, since these studies are very similar in approach. In addition to our model described above (the "baseline" run), we have carried out a "Gruber-TM3" model run. In this run, we combine the air-sea O_2 fluxes of Gruber '01 with TM3, rather than GCTM. We also use the appropriate years of fossil fuel input (see Table 1). Results of the baseline and

Table 1. Models and Fluxes Used in This Work and Earlier Studies[a]

Input Fluxes and Transport Model	*Stephens et al.* [1998]	*Gruber et al.* [2001]	This Study
Fossil fuel O_2 and CO_2	*Marland et al.* [1985], *Andres et al.* [1998]	*Marland et al.* [1998]	*Marland et al.* [2003]
Oceanic pCO_2	various OBMs	*Takahashi et al.* [1999]	*Takahashi et al.* [1999]
Oceanic seasonal O_2	various OBMs	*Najjar and Keeling* [2000]	*Garcia and Keeling* [2001]
Oceanic seasonal N_2	various OBMs	*Esbensen and Kushnir* [1981]	*Garcia and Keeling* [2001]
Oceanic annual mean O_2	various OBMs	*Gruber et al.* [2001]	*Gruber et al.* [2001]
Oceanic annual mean N_2	various OBMs	*Gloor et al.* [2001]	*Gloor et al.* [2001]
Atmospheric transport model	TM2	GCTM	TM3

[a]"OBM" refers to the ocean biogeochemistry models considered in the *Stephens et al.* [1998] study.

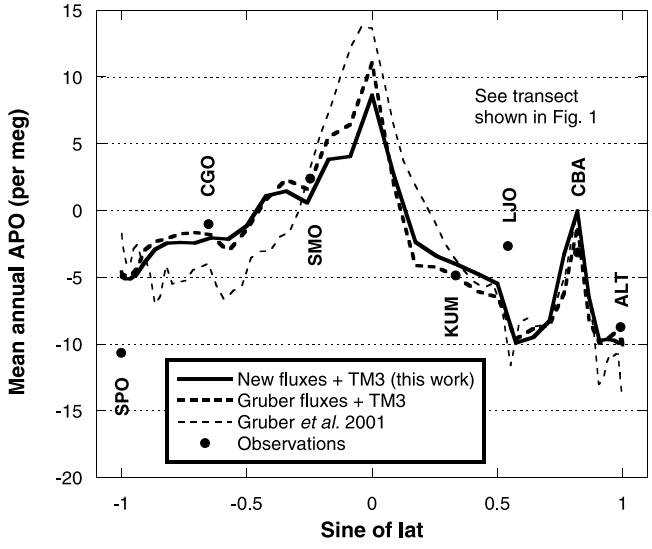

Figure 7. Modeled values of mean annual APO along the transect shown in Figure 1. Model runs include the KVLOW(h) run from *Gruber et al.* [2001], the same air-sea gas fluxes, but with the TM3 model of atmospheric transport (Gruber-TM3), and updated seasonal O_2 and N_2 oceanic fluxes with the TM3 model (this work/baseline). See Table 1 for complete descriptions. Also shown are annual average measurements of APO at the land stations that lie along the specified transect (observations). These observations are identical to the closed symbols shown in panel 4 of Figure 2. Because zero-points are arbitrary for the models, all model curves have been shifted agree optimally with the observations (in a least squares sense). The baseline model results shown here differ from the model curves in Figure 2 only in the spatial sampling and time averaging of the model output.

Gruber-TM3 runs are shown in Figure 7, along with the original result from the Gruber '01 manuscript.

[59] A comparison of the baseline and Gruber-TM3 model runs reveals that our choice of seasonal O_2 and N_2 flux fields has very little impact on the north-south gradient. Annual mean values at the land stations change by 1 per meg or less, and equatorial values agree within 2 per meg. While the *Garcia and Keeling* [2001] O_2 and N_2 fluxes used in the baseline run are almost certainly closer to the truth than those of *Najjar and Keeling* [2000] used in the Gruber-TM3 run, the north-south gradient is largely insensitive to the difference between these two estimates of seasonal air-sea fluxes.

[60] In addition, we can compare the Gruber-TM3 run with the original Gruber '01 result (the heavy and light dashed lines in Figure 7). The SPO-ALT gradients for these two model runs differ by 5.8 per meg. Note that for this figure, we have extracted annual mean values from the three model runs along exactly the same transect as used by Gruber '01. Thus the differences between these two curves reflect only different transport models (TM3 and GCTM), and different periods of fossil fuel input. The different periods used for the fossil fuel input probably change interhemispheric APO gradients by $\sim$1 per meg or less. Therefore we conclude that the difference in interhemispheric gradients calculated by the Gruber '01 study and this work is due almost entirely to the choice of atmospheric transport model. Although this comparison highlights the importance of the atmospheric transport model, we remain unable to say which model (if either) is accurately characterizing the true atmosphere.

[61] While our baseline model run shows excellent agreement with the data, if our data set instead covered the same years as Stephens '98, we too would see a data-model mismatch since the observations show a strong temporal dependence in the north-south gradient. Until we understand the causes of the variation in this gradient, the time-averaged quantity will remain of limited utility in assessing the relative strengths of competing models.

6.2. Equatorial Bulge

[62] One of the most dramatic features predicted by the models in the original work of Stephens '98 was the existence of a prominent maximum in APO in the tropics (the"equatorial bulge"). This bulge was common to all models tested, and was also predicted by Gruber '01. The bulge results from low-latitude outgassing of O_2 and CO_2. This outgassing arises from the equatorial upwelling of cold waters rich in nutrients and CO_2 but low in O_2. The ventilation of these waters leads to an influx of O_2 in the immediate vicinity of the equator. As the waters flow poleward, they are rapidly resaturated, after which the continuing biological consumption of their nutrient burden and steady warming lead to a substantial O_2 efflux. It is this O_2 efflux, along with a CO_2 efflux resulting from the high pCO_2 and the warming of the upwelled water (and the relatively slow air-sea exchange of CO_2), that result in the equatorial bulge in APO. The magnitude of the bulge depends upon the vigor of equatorial upwelling, the heat flux (which diminishes O_2 and CO_2 solubility, driving both gases into the atmosphere), the concentrations of O_2, nutrients and CO_2 in the upwelled water, and the rate at which atmospheric transport disperses the air-sea gas fluxes (Stephens '98 and Gruber '01).

[63] Our new results from shipboard sampling (panels 3 and 4 of Figure 2) show that this equatorial bulge is a prominent feature in the data. APO values clearly increase toward the equator, both north of Samoa (SMO) and south of Cape Kumukahi (KUM). The highest values of APO occur just south of the Equator, but this asymmetry is not statistically significant. Peak values are 5–8 per meg higher than SMO and 13–16 per meg higher than KUM (depending on analysis method). The data do, however, show that the bulge clearly extends farther to the south than to the north (compare means at 10°N and 10°S).

[64] Also shown in panels 3 and 4 of Figure 2 are our model results. A similar feature is clearly evident in the model output, with maximum APO values just south of the equator. We have not yet examined these model results in detail, but believe that two features contribute to the greater southward extent of the bulge. First, the climatological ITCZ is in the Northern Hemisphere, so that equatorial upwelling will have a greater impact on Southern Hemi-

sphere air. Second, the equatorial upwelling zone lies south of the equator in the eastern equatorial Pacific. Surprisingly, the model bulge is substantially smaller than observed, with a peak that is only 2–5 per meg higher than SMO and 9–11 per meg higher than KUM.

[65] There are at least two possible causes for the data-model discrepancy in the size of the bulge. First, the modeled transport in the atmosphere may be too vigorous, either poleward or vertically. If so, the calculated peak will be attenuated. Second, as discussed by Gruber '01, the regions for which the air-sea O_2 fluxes are determined are probably too coarse to allow the atmospheric transport model to capture the detailed structure of O_2 in the immediate vicinity of the equator.

[66] On the other hand, several aspects of the model bulge appear robust. Because the model bulge results from roughly equal contributions from CO_2 and O_2 outgassing (Gruber '01), the prediction will not be particularly sensitive to errors in the ocean GCM used to determine the annually averaged air-sea fluxes. As shown by Gruber '01, an ocean model which yields very vigorous equatorial oxygen efflux leads to only a modest increase in the equatorial bulge. Furthermore, the CO_2 fluxes for the Tropical Pacific are well constrained, thanks to an abundance of ΔpCO_2 data in this region [*Takahashi et al.*, 1999].

[67] Figure 7 shows the degree to which the choice of atmospheric transport model determines the size and shape of the bulge. The "Gruber-TM3" and "Gruber 2001" model runs differ only in the choice of transport model (TM3 and GCTM, respectively). The difference between them clearly shows that the relatively sluggish transport of GCTM makes the peak somewhat higher relative to KUM and SMO and dramatically lowers APO at all latitudes south of SMO. In contrast, the agreement of the "baseline" and "Gruber-TM3" runs shows that the size of the bulge is insensitive to the choice of seasonal O_2 and N_2 fluxes (see section 6.1 and Table 1 for model descriptions).

6.3. Northern Extratropical Gradients

[68] In addition to the interhemispheric gradient and the equatorial bulge, Figure 2 reveals some structure in the extratropical APO gradients. The model predicts some of this structure, but not all. Owing to sparse oceanic data in the high southern latitudes, it is hard to assess the robustness of the southern extratropical gradients. In this section, we examine the more robust features in the northern extratropical APO gradients.

[69] Panels 3 and 4 of Figure 2 show that the model does an excellent job of predicting the KUM-ALT gradient, while the data-model discrepancy in the BRW-ALT gradient is roughly within measurement uncertainties. The model gives a value that is 6 per meg too high for CBA, relative to the other two sites. This is probably due to excessive trapping of a brief and local marine signal by the atmospheric transport model (see section 6.4). Uncertainties in the shipboard observations preclude meaningful comparisons at 20°N and 30°N.

[70] Thus the primary data-model discrepancy to examine in the Northern extratropics is the model prediction of APO values at LJO and SAB that are ~4 per meg lower than observations, relative to the KUM-ALT gradient. A simple bias in the data seems unlikely since neither station has a particularly large Ar/N_2 correction factor. The LJO record has very little scatter and data are abundant. The SAB record is of poorer quality, with some substantial gaps due to problems with collection equipment, but the data are still abundant enough to define an accurate annual mean value (see Figures 2, 3, and 5).

[71] One possible explanation for the data-model disagreement at LJO relative to KUM and ALT is selective sampling of the atmosphere at LJO. Samples are collected from the end of the Scripps Pier at LJO only when the wind is from the west in an effort to avoid the substantial anthropogenic signal originating from the urban areas to the East. No effort has been made to emulate this sampling protocol in the model. An east-west gradient in model APO implies that if the selective sampling protocol at LJO effectively translates the site westward, the data-model discrepancy could be resolved.

[72] This hypothesis is consistent with the data-model discrepancy in the seasonal cycle at LJO (Figure 5). The annual mean APO at LJO is lower because the summer peak predicted by the model is too low, even though the winter trough is correct. Furthermore, the modeled increase in APO to the West of LJO steepens significantly during the summer. Thus it seems likely that if we were to selectively sample air originating from the West of LJO when conducting the model analysis, we might well resolve the data-model discrepancies in both the annual mean value and the shape of the seasonal cycles. This is clearly only a working hypothesis at this point, as we cannot rule out more substantive problems with model fluxes, transport, or a bias in the observations.

[73] The discrepancy at Sable Island (SAB) is harder to explain. Because there is essentially no sector selection in place at Sable Island, our working hypothesis for LJO doesn't apply. Without an effort well beyond the scope of this paper, we cannot say whether the data-model difference at SAB is due to errors in the O_2 and CO_2 flux fields, the modeled atmospheric transport, or a bias in the data itself.

6.4. Seasonal Cycles

[74] North-south gradients in APO are not the only metric for comparing model results with observations. The model should also correctly predict the amplitude and phasing of the seasonal cycles of APO over a wide geographic range. The seasonal cycle is a particularly useful metric since it is nearly immune to the complications that affect the measurement of spatial gradients (such as the intranetwork biases discussed above). Figure 5 shows the observed climatological cycle at the land stations and the model output.

[75] In general, the modeled values are quite close to the observations. The most obvious disagreement occurs at Cold Bay (CBA), where the model shows a much more pronounced APO maximum. In addition to the discrepancy at CBA, the model underpredicts the magnitude of the cycle slightly at La Jolla (LJO) and Barrow (BRW), and overpredicts it slightly at Palmer Station (PSA), Syowa (SYO), and South Pole (SPO).

[76] We can gain some understanding of these discrepancies by comparing our data-model differences with those found by *Garcia and Keeling* [2001]. These authors used exactly the same seasonal O_2 and N_2 fluxes to drive a model of atmospheric transport and then compared the predicted seasonal cycles with the observed APO at many of the stations we consider here. To simulate atmospheric transport, *Garcia and Keeling* [2001] used TM2, an earlier version the TM3 model we employ. These two models have significantly different performance [*Heimann*, 1995; *Heimann and Körner*, 2003; *Gurney et al.*, 2003].

[77] Consider first CBA. As calculated by the model, there is a region of very high APO that briefly covers the Bering Sea during the month of July. This high APO appears to arise from a large oceanic O_2 efflux in the immediate vicinity [*Garcia and Keeling*, 2001]. The presence of a strong ocean CO_2 sink at roughly the same time and place [*Takahashi et al.*, 2002] implies that a seasonal upwelling event (with accompanying nutrient flux and subsequent bloom) may be the underlying cause of the O_2 efflux and resulting spike in APO. Garcia and Keeling found better agreement between the observed and predicted APO cycles at CBA than we do, with no sign of a spurious summer maximum in the model. Thus differences in calculated APO at CBA result from differences in transport between TM2 and TM3. The TM3 model has been shown in other studies to overestimate tracer concentrations near source regions [*Denning et al.*, 1999], suggesting that this model has excessive vertical trapping. Our results are consistent with this suggestion.

[78] At LJO and SPO, *Garcia and Keeling* [2001] found data-model discrepancies of roughly the same size as we observe, suggesting that, at these sites, the problem may come from estimates of seasonal O_2 and N_2 fluxes, as well as errors in model transport.

7. Summary

[79] When appropriately combined, measurements of atmospheric O_2 and CO_2 can be used to gain insight into air-sea gas transfer, ocean biogeochemistry, and atmospheric transport. Building on the earlier work of Stephens '98, we have used measurements of O_2 and CO_2 from the Princeton and Scripps flask sampling networks and NOAA/CMDL to create a global record of atmospheric potential oxygen. One of the distinguishing features of this record is new coverage in the equatorial Pacific.

[80] From these records, we have derived a climatology of the annual mean north-south gradient in APO using two different methods to fill in spatiotemporal gaps in our data set. We have also used measurements of the atmospheric Ar/N_2 ratio to reduce the impact of collection biases on our data set.

[81] Compared to earlier APO studies, we find a smaller interhemispheric gradient. We attribute this difference primarily to different periods of averaging in the context of the ongoing evolution of this gradient. Our data also show an unequivocal maximum in APO at low latitudes (the "equatorial bulge"), a feature predicted in earlier modeling studies.

[82] We have also modeled APO fields, using an updated version of the method developed by Gruber '01. The gradients of APO predicted by this method generally agree with our observations. The predicted interhemispheric gradient is within ~4 per meg of observations, in contrast to earlier studies, in which the models significantly underpredicted the gradient. We attribute the resolution of this discrepancy primarily to real changes in the APO distribution over time: The observed APO gradient has changed to the point that it is now compatible with the models we employ. Despite being driven by interannually varying winds, there is nothing in these models that predicts a secular change in the APO gradient. This highlights the importance of a deeper understanding of the processes that determine the APO gradient.

[83] The observed APO maximum in the tropics is also predicted by our model, with agreement in the north-south extent, but an underprediction of the amplitude. The modeled value of this feature depends strongly upon the details of the atmospheric transport model. In particular, the TM3 model we employ appears to vigorously transport the strong equatorial APO efflux into the southern subtropics and subpolar region, thereby reducing the tropical maximum (perhaps too much) while elevating APO in the southern extratropics to levels that agree well with observations. Finally, in the northern extratropics, the modest data-model mismatch at La Jolla may be explained by our failure to impose realistic wind-sector selection criteria when recording model output.

[84] The seasonal air-sea flux fields of *Garcia and Keeling* [2001], together with the TM3 atmospheric tracer transport model, do a fine job of reproducing the seasonal cycles of APO at most stations. Only at Cold Bay is the cycle poorly predicted, most probably owing to excessive trapping of the summer APO signal by the TM3 atmospheric transport model we employ. Smaller data-model differences at La Jolla and South Pole are more likely due to errors in the seasonal cycles of air-sea APO fluxes that are used to drive the atmospheric transport model.

[85] On the basis of the data set in hand, our ability to generally match the observations with modeled values, and comparison of our model results with those already published, we conclude that north-south gradients in APO are sensitive to a range of important processes that are simulated differently in different models of atmospheric transport. The predicted gradients will certainly also depend on the air-sea fluxes of APO that are used as a lower boundary condition for the atmospheric transport models. Nonetheless, until the present uncertainties in atmospheric transport are significantly reduced, we will not be in a position to quantitatively assess the quality of air-sea flux estimates.

[86] We look forward to continued improvement in data coverage and quality, both temporally and spatially. With longer records, we will have the opportunity to determine the factors that control interannual variations in the APO gradients we have characterized. Better spatial coverage, particularly beyond the Pacific basin, will improve our ability to test zonal transport and vertical mixing over continents in atmospheric transport models and make our test of air-sea flux fields far more stringent. Finally, reduc-

tion in site-to-site biases through improved and automated collection equipment will strengthen all of the analyses presented here.

[87] **Acknowledgments.** We thank the staffs of the observatories and the sailors of the merchant and scientific vessels for their careful collections and generous efforts. Cape Grim and MacQuarie data are collected under the umbrella of the CSIRO Atmospheric Research Program (in collaboration with R. J. Francey and R. L. Langenfelds) supported by the Australian Bureau of Meteorology and the Australian Antarctic Division. Back-trajectory analyses were graciously provided by Joyce Harris of NOAA/CMDL and we thank Martin Heimann for the use of his TM3 model. This work was supported by the National Science Foundation under grants 9601722, 9601722, 0000923, 0330096, ATM-0350719, and ATM-9911319, and NOAA Office of Global Programs under grant NA77RJ0453A. Any opinions, findings, and conclusions or recommendations expressed in this material are those of the authors and do not necessarily reflect the views of the National Science Foundation. Additional support was provided by the The Princeton/BP Amoco Carbon Mitigation Initiative.

References

Andres, R., G. Marland, T. Boden, and S. Bischoff (1998), Carbon dioxide emissions from fossil fuel combustion and cement manufacture 1751–1991 and an estimate of their isotopic composition and latitudinal distribution, in *1993 Global Change Institute*, edited by T. Wigley and D. Schimel, Cambridge Univ. Press, New York.

Battle, M., M. L. Bender, P. Tans, J. White, J. Ellis, T. Conway, and R. Francey (2000), Global carbon sinks and their variability inferred from atmospheric O_2 and $\delta^{13}c$, *Science*, *287*, 2467–2470.

Battle, M., M. Bender, M. B. Hendricks, D. T. Ho, R. Mika, G. McKinley, S.-M. Fan, T. Blaine, and R. F. Keeling (2003), Measurements and models of the atmospheric Ar/N_2 ratio, *Geophys. Res. Lett.*, *30*(15), 1786, doi:10.1029/2003GL017411.

Bender, M. L., P. P. Tans, J. T. Ellis, J. Orchardo, and K. Habfast (1994), A high precision isotope ratio mass spectrometry method for measuring the O_2/N_2 ratio of air, *Geochim. Cosmochim. Acta*, *58*(21), 4751–4758.

Bender, M., T. Ellis, P. Tans, R. Francey, and D. Lowe (1996), Variability in the O_2/N_2 ratio of Southern Hemisphere air, 1991–1994: Implications for the carbon cycle, *Global Biogeochem. Cycles*, *10*(1), 9–21.

Bender, M. L., D. T. Ho, M. B. Hendricks, R. Mika, M. O. Battle, P. P. Tans, T. J. Conway, B. Sturtevant, and N. Cassar (2005), Atmospheric O_2/N_2 changes, 1993–2002: Implications for the partitioning of fossil fuel CO_2 sequestration, *Global Biogeochem. Cycles*, *19*, GB4017, doi:10.1029/2004GB002410.

Conway, T. J., P. P. Tans, L. S. Waterman, K. W. Thoning, D. R. Kitzis, K. A. Masarie, and N. Zhang (1994), Evidence for interannual variability of the carbon cycle from the National Oceanic and Atmospheric Administration/Climate Monitoring and Diagnostics Laboratory global air sampling network, *J. Geophys. Res.*, *99*(D11), 22,831–22,855.

Denning, S. A., et al. (1999), Three-dimensional transport and concentration of SF6: A model intercomparison study (transcom 2), *Tellus, Ser. B*, *51*, 266–297.

Esbensen, S., and J. Kushnir (1981), The heat budget of the global oceans: An atlas based on estimates from marine surface observations, *Tech. Rep. 29*, Clim. Res. Inst., Oreg. State Univ., Eugene.

Garcia, H. E., and R. F. Keeling (2001), On the global oxygen anomaly and air-sea flux, *J. Geophys. Res.*, *106*(C12), 31,155–31,166.

Gloor, M., N. Gruber, T. M. Hughes, and J. L. Sarmiento (2001), An inverse modeling method for estimation of net air-sea fluxes from bulk data: Methodology and application to the heat cycle, *Global Biogeochem. Cycles*, *15*(4), 767–782.

Gruber, N., M. Gloor, S.-M. Fan, and J. L. Sarmiento (2001), Air-sea flux of oxygen estimated from bulk data: Implications for the marine and atmospheric oxygen cycles, *Global Biogeochem. Cycles*, *15*(4), 783–803.

Gurney, K., R. Law, P. Rayner, and A. Denning (2000), TRANSCOM3 experimental protocol, *Tech. Rep. 707*, Dep. of Atmos. Sci., Colo. State Univ., Fort Collins. (Available at http://transcom.colostate.edu/TransCom_3)

Gurney, K., et al. (2003), TRANSCOM 3 CO_2 inversion intercomparison: 1. Annual mean control results and sensitivity to transport and prior flux information, *Tellus, Ser. B*, *55*, 555–579.

Heimann, M. (1995), The global atmospheric tracer model TM2, *Tech. Rep. 10*, Dtsch. Kimarechenzentrum, Hamburg, Germany.

Heimann, M., and S. Körner (2003), The global atmospheric tracer model TM3: Model description and user's manual, technical report, Max-Planck-Inst. für Biogeochem., Jena, Germany.

Kalnay, E., et al. (1996), The NCEP/NCAR 40-year reanalysis project, *Bull. Am. Meteorol. Soc.*, *77*, 437–471.

Keeling, R. F. (1988a), Development of an interferometric oxygen analyzer for precise measurement of the atmospheric O_2 mole fraction, Ph.D. thesis, Harvard Univ., Cambridge, Mass.

Keeling, R. F. (1988b), Measuring correlations between atmospheric oxygen and carbon dioxide mole fractions: A preliminary study in urban air, *J. Atmos. Chem.*, *7*, 153–176.

Keeling, R. F., and S. R. Shertz (1992), Seasonal and interannual variations in atmospheric oxygen and implications for the global carbon cycle, *Nature*, *358*, 723–727.

Keeling, R. F., S. C. Piper, and M. Heimann (1996), Global and hemispheric CO_2 sinks deduced from changes in atmospheric O_2, *Nature*, *381*, 218–220.

Keeling, R., A. Manning, E. McEvoy, and S. Shertz (1998), Methods for measuring changes in atmospheric O_2 concentration and their application in Southern Hemisphere air, *J. Geophys. Res.*, *103*(D3), 3381–3397.

Keeling, R. F., T. Blaine, B. Paplawsky, L. Katz, C. Atwood, and T. Brockwell (2004), Measurments of changes in atmospheric Ar/N_2 ratio using a rapid-switching, single-capillary mass spectrometer system, *Tellus, Ser. B*, *56*(4), 322–338.

Mahlman, J. D., and W. J. Moxim (1978), Tracer simulation using a global general circulation model: Results from a mid-latitude instaneous source experiment, *J. Atmos. Sci.*, *35*, 1340–1374.

Manning, A. C. (2001), Temporal variability of atmospheric oxygen from both continuous measurements and a flask sampling network: Tools for studying the global carbon cycle, Ph.D. thesis, Univ. of Calif., San Diego, La Jolla.

Marland, G., R. Rotty, and N. Treat (1985), CO_2 from fossil fuel burning: Global distribution of emissions, *Tellus, Ser. B*, *37*, 243–258.

Marland, G., R. Andres, T. B. C. Johnston, and A. Brenkert (1998), Global, regional and national CO_2 emission estimates from fossil fuel burning, cement production and gas flaring: 1751–1996 (revised August 2000), *Data Rep. ORNL NDP-030*, Carbon Dioxide Inf. Anal. Cent., Oak Ridge Natl. Lab., Oak Ridge, Tenn.

Marland, G., T. Boden, and R. Andres (2003), Global, regional and national CO_2 emissions, in *Trends: A Compendium of Data on Global Change*, Carbon Dioxide Inf. Anal. Cent., Oak Ridge Natl. Lab., U.S. Dep. of Energy, Oak Ridge, Tenn.

Najjar, R., and R. Keeling (2000), Mean annual cycle of the air-sea oxygen flux: A global view, *Global Biogeochem. Cycles*, *14*(2), 573–584.

Severinghaus, J. P. (1995), Studies of the terrestrial O_2 and carbon cycles in sand dune gases and in Biosphere 2, Ph.D. thesis, Columbia Univ., New York.

Stephens, B. B. (1999), Field-based atmospheric oxygen measurements and the ocean carbon cycle, Ph.D. thesis, Univ. of California, San Diego, La Jolla.

Stephens, B. B., R. F. Keeling, M. Heimann, K. D. Six, R. Murnane, and K. Caldeira (1998), Testing global ocean carbon cycle models using measurements of atmospheric O_2 and CO_2 concentration, *Global Biogeochem. Cycles*, *12*(2), 213–230.

Takahashi, T., R. Wanninkhof, R. Feely, R. Weiss, D. Chipman, N. Bates, J. Olafsson, C. Sabine, and S. Sutherland (1999), Net sea-air CO_2 flux over the global oceans: An improved estimate based on the sea-air pCO_2 difference, paper presented at 2nd International Symposium on CO_2 in the Oceans, Natl. Inst. for Environ. Stud., Tsukuba, Japan.

Takahashi, T., et al. (2002), Gobal sea-air CO_2 flux based on climatological surface ocean pCO_2, and seasonal biological and temperature effects, *Deep Sea Res., Part II*, *49*(9–10), 1601–1622.

Tans, P. P., T. Conway, and T. Nakazawa (1989), Latitudinal distribution of the sources and sinks of atmospheric carbon-dioxide derived from surface observations and an atmospheric transport model, *J. Geophys. Res.*, *94*(D4), 5151–5172.

Thoning, K. W., P. P. Tans, and W. D. Komhyr (1989), Atmospheric carbon dioxide at Mauna Loa observatory: 2. analysis of the NOAA GMCC data, 1974–1985, *J. Geophys. Res.*, *94*(D6), 8549–8565.

Tohjima, Y., H. Mukai, T. Machida, and Y. Nojiri (2003), Measurements of atmospheric O_2/N_2 ratio from two monitoring stations in Japan and shipboard sampling in the western and northern Pacific region, *Geochim. Cosmochim. Acta*, *67*(18), A483.

M. Battle, Department of Physics and Astronomy, Bowdoin College, 8800 College Station, Brunswick, ME 04011, USA. (mbattle@bowdoin.edu)

M. L. Bender, M. B. Hendricks, and R. Mika, Department of Geosciences, Guyot Hall, Princeton University, Princeton, NJ 08544, USA.

S. M. Fletcher and N. Gruber, Institute of Geophysics and Planetary Physics and Department of Atmospheric and Oceanic Sciences, University of California, Los Angeles, CA 90095, USA.

D. T. Ho, Lamont-Doherty Earth Observatory, Columbia University, Palisades, NY 10964, USA.

R. F. Keeling and B. Paplawsky, Scripps Institution of Oceanography, University of California, San Diego, La Jolla, CA 92093-0236, USA.

A. C. Manning, School of Environmental Sciences, University of East Anglia, Norwich NR4 7TJ, UK.

C. Simonds, Canaccord Adams, 99 High Street, 11th Floor, Boston, MA 02110, USA.

P. P. Tans, National Oceanic and Atmospheric Administration, Climate Monitoring and Diagnostics Laboratory, Boulder, CO 80303, USA.